Title

Side chain length affects backbone dynamics in poly(3-alkylthiophene)s

Authors

Zhan, Pengfei

Zhang, Wenlin

Jacobs, Ian E

et al.

Peer reviewed

Side Chain Length Affects Backbone Dynamics in Poly(3-Alkylthiophene)s

Pengfei Zhan,[1] Wenlin Zhang,[1] Ian E. Jacobs,[2] David M. Nisson,[3] Renxuan Xie,[1]
Albree R. Weissen,[1] Ralph H. Colby,[1,4] Adam J. Moulé,[3] Scott T. Milner,[1,4] Janna K. Maranas,[1,4]
Enrique D. Gomez ⓘ[1,4,5]

[1]Department of Chemical Engineering, The Pennsylvania State University, University Park, Pennsylvania
[2]Department of Materials Science and Engineering, University of California, Davis, California
[3]Department of Chemical Engineering, University of California, Davis, California
[4]Department of Material Science and Engineering, The Pennsylvania State University, University Park, Pennsylvania
[5]Materials Research Institute, The Pennsylvania State University, University Park, Pennsylvania
Correspondence to: E. D. Gomez (E-mail: edg12@psu.edu)

ABSTRACT: Charge transport in conjugated polymers may be governed not only by the static microstructure but also fluctuations of backbone segments. Using molecular dynamics simulations, we predict the role of side chains in the backbone dynamics for regiorandom poly(3-alkylthiophene-2,5-diyl)s (P3ATs). We show that the backbone of poly(3-dodecylthiophene-2-5-diyl) (P3DDT) moves faster than that of poly(3-hexylthiophene-2,5-diyl) (P3HT) as a result of the faster motion of the longer side chains. To verify our predictions, we investigated the structures and dynamics of regiorandom P3ATs with neutron scattering and solid state NMR. Measurements of spin-lattice relaxations (T_1) using NMR support our prediction of faster motion for side chain atoms that are farther away from the backbone. Using small-angle neutron scattering (SANS), we confirmed that regiorandom P3ATs are amorphous at about 300 K, although microphase separation between the side chains and backbones is apparent. Furthermore, quasi-elastic neutron scattering (QENS) reveals that thiophene backbone motion is enhanced as the side chain length increases from hexyl to dodecyl. The faster motion of longer side chains leads to faster backbone dynamics, which in turn may affect charge transport for conjugated polymers. © 2018 Wiley Periodicals, Inc. J. Polym. Sci., Part B: Polym. Phys. **2018**

KEYWORDS: conjugated polymers; charge transport; quasi elastic neutron scattering; side chain motion; solid state NMR

INTRODUCTION Semiconducting conjugated polymers, such as poly(3-alkylthiophene-2,5-diyl)s (P3ATs), are promising materials for next-generation flexible electronics.[1–4] Fully conjugated backbones composed of aromatic moieties, such as thiophene and benzothiophene, can lead to intramolecular charge delocalization along the backbone and strong coupling between chains.[5–9] As a consequence, electrons and holes can transport intra- and inter-molecularly through thermally activated hopping processes.[10,11] For conjugated polymers, the electronic coupling between different backbone moieties and the resulting hopping efficiency depend strongly on the static local order.

Molecular motions of conjugated polymers can lead to fluctuations in local structures, such as π–π stacking distances and backbone dihedral angles, which in turn affect charge transport.[12–16] For example, the vibrations of polymer backbones in the π–π stacking direction can result in fluctuations of intermolecular electronic couplings. Conformational fluctuations,

resulting from backbone motions, may also enhance intra-chain charge transfer by releasing "traps" (twisted rings) along chain backbones.[17]

Investigating the effect of molecular structure on the backbone dynamics is therefore crucial for understanding charge transport in conjugated polymers. The properties of molecular motion, however, have not been intensively studied.[18,19] Direct measurements of the chain dynamics of conjugated polymer backbones are challenging.

In this work, we combine atomistic molecular dynamics (MD) simulations, solid-state NMR, small angle neutron scattering (SANS), and quasi-elastic neutron scattering (QENS) to investigate the effect of side chain length on the dynamics of three regiorandom poly(3-alkylthiophene-2,5-diyl)s (P3ATs): poly(3-hexylthiophene-2,5-diyl) (P3HT), poly(3-octylthiophene-2,5-diyl) (P3OT), and poly(3-dodecylthiophene-2,5-diyl)

Additional Supporting Information may be found in the online version of this article.
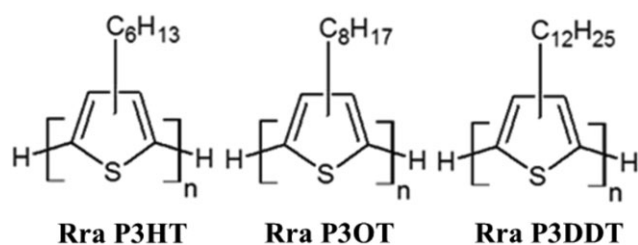
FIGURE 1 Chemical structures of regiorandom poly (3-hexylthiophene-2,5-diyl), poly(3-octylthiophene-2,5-diyl), and poly(3-dodecylthiophene-2,5-diyl) from left to right.

(P3DDT) (Fig. 1). We chose regiorandom P3ATs as model materials because they are amorphous at room temperature. In this way, we avoid the complications in the measurements of chain dynamics that may arise from the existence of crystalline domains for semicrystalline regioregular polymers.

In MD simulations, we directly measured the mean-square displacements of the atoms on P3HT and P3DDT. We show that the side chain atoms can move faster than the backbone atoms. We also predict that by changing the side chain length from hexyl to dodecyl, the backbone motion is enhanced for regiorandom P3ATs.

To validate our predictions, we also obtained the dynamical properties of regiorandom P3HT, P3OT, and P3DDT from neutron scattering experiments. Using SANS, we observe that the regiorandom P3ATs are amorphous at 300 and 350 K, although the high q peaks in the SANS spectra indicate the existence of disordered lamellar structures. Solid state NMR results for regiorandom P3HT show that the motion of the side chain carbons is enhanced away from the backbone. Furthermore, using QENS, we reveal the dynamics of hydrogen atoms in the three P3ATs. We demonstrate that the amplitude of motions for protons on the thiophene rings indeed increases as the side chain length increases from hexyl to dodecyl.

Our results may help explain the dependence of performance on side chain length for conjugated polymers. For example, our TFT measurements suggest that charge mobilities of regiorandom P3ATs decrease as side-chain length increases (discussed in the Supporting Information Fig. S1 and Supporting Information Table S1). Previous studies also show that material performance is related to the side chain length for regioregular polymers.[14,15,20,21] Because the side chains are not conductive[22] and the π–π stacking spacing is roughly the same for conjugated polymers that differ only in side chain length,[23] the difference in performance may arise from the different dynamics of polymer backbones.

EXPERIMENTAL

Materials
Regiorandom poly(3-hexylthiophene-2,5-diyl) (P3HT), poly (3-octylthiophene-2,5-diyl) (P3OT), and poly(3-dodecylthio-phene-2,5-diyl) (P3DDT) were purchased from Sigma Aldrich. The polymers were re-precipitated in cold methanol and extensively purified by Soxhlet extraction with acetone and methanol as previously described.[24]

Differential Scan Calorimetry
The glass transition temperature T_g and other thermal transitions of P3ATs were measured by TA Q2000 differential scanning calorimetry (DSC). The scans were performed over a temperature range from −70 to 250°C at a rate of 5°C/min. For each sample, the first heating/cooling cycle was used to eliminate the thermal history in the material. Only data from the second cycle was used for analysis.

Small Angle Neutron Scattering
Samples for SANS experiment were pressed between Teflon slabs at 350 K with a Carver laboratory press. The final film thickness is around 200 μm. Small angle neutron scattering (SANS) experiments were performed to characterize the structural properties of P3ATs using Extended Q-range Small Angle Neutron Scattering Spectrometer (EQ-SANS) at the Spallation Neutron Source (SNS), Oak Ridge National Lab in Oak Ridge, TN.[25] In order to achieve an effective q-range of 0.005–1 Å ([$q = 4\pi\sin(\theta/2)/\lambda$], where θ is the scattering angle), the sample-detector distance and incident neutron wave length λ were varied from 1.3 to 6 m and 10 and 2.5 Å, respectively. The quality of data was improved by performing background subtraction and detector efficiency correction using MantidPlot.

Quasi-Elastic Neutron Scattering
Samples for QENS experiment were wrapped in aluminum foil and pressed at 450 K. Samples were 60 μm in thickness to prevent multiple scattering (10% scattering at this thickness). In order to eliminate the uptake of water, the samples were loaded into Aluminum HFBS annular sample cans in a dry helium atmosphere and sealed with an indium O-ring for subsequent QENS measurements.

The proton dynamics in regiorandom P3ATs were measured using QENS. Protons have significantly larger incoherent scattering cross sections than C and S atoms, and in turn contribute to more than 90% of incoherent scattering signal.[26] Using fixed window scans, we observed the transitions in dynamics when the temperatures were high enough to activate segmental motions for P3ATs. We also performed dynamic scans for P3ATs at 300 and 350 K, where the side chains were mobile. From the dynamic scans, we obtained the scattering function S(q,ω), which characterized the self-diffusive motions of the protons. By analyzing S(q,ω), we extracted the elastic incoherent structure factor (EISF).[27,28] By fitting EISF, we computed the amplitude of proton motions in P3ATs.

QENS experiments were performed using the high-flux backscattering spectrometer (HFBS) at the National Institute of Standards and Technology Center for Neutron Research in Gaithersburg, MD.[29] Fixed window scans (FWS) were performed on HFBS with the Doppler drive at rest. The scans cover a temperature range from 100 to 450 K with a rate of 0.5 K/min. The incoherent elastic signals were collected at 16 different wave vectors ranging between 0.23 and 1.75 Å^{-1}

as a function of temperature. In dynamic scans, the incident neutron wave had a wavelength of about 6.271 Å (E = 2.08 meV) after passing the monochromator drive system (Doppler). The scattered neutrons with energy of 2.08 meV were selectively reflected to detector by Si(1,1,1) analyzer crystals. The dynamic scans range from −17 to + 17 μeV and the energy resolution (minimal neutron energy change that can be detected by the instrument) was 0.8 μeV. The incoherent quasi-elastic signals were collected as a function of change in neutron energy at 300 and 350 K. Data was corrected for detector efficiency and the background was subtracted using DAVE software, developed by the National Institute of Standard and Technology Center.[30]

The instrument resolution was measured using vanadium foil at room temperature. All the other measurement conditions are the same as samples. To calculate the intermediate scattering function, we inverse Fourier transform experimental data $I(q,\omega)$ and resolution $R(q,\omega)$ to obtain $I(q,t)$ and $R(q,t)$. $I(q,t)$ and $R(q,t)$ is then normalized by the value at t = 0 giving $I^{norm}(q,t)$ and $R^{norm}(q,t)$. The intermediate scattering function $S(q,t)$ is then the ratio $I^{norm}(q,t)/R^{norm}(q,t)$.

Molecular Dynamics Simulations

We performed atomistic MD simulations to investigate the role of side chains on the dynamics of P3AT backbones. Using simulations, we directly measured the motions of atoms on the side chains and the backbones for P3ATs, which were later compared with QENS experiments.

We simulated regiorandom P3HT and P3DDT using the GROMACS package.[31] The force field model was developed by Huang and co-workers for regioregular P3HT.[32,33] The bonded interactions and the partial charges were obtained using density functional theory (DFT) calculations. The Lennard–Jones (LJ) parameters were borrowed from the OPLS-AA model.[34] Huang et al. validated the atomistic model by comparing the densities of 3-hexylthiophene and crystalline regioregular P3HT to experiments. We have also demonstrated that this force field model could yield chain dimensions and nematic phase behavior that were consistent with experiments for regioregular P3HT.[35–38] We expect the atomistic model is also valid for other P3ATs, including the regiorandom chains, which only differ from regioregular P3HT in side chain length and regioregularity.

Each initial configuration of our simulations was composed of 64 chains of loosely packed regiorandom P3AT 20mers. The regiorandom chains were generated by randomly connecting two types of P3AT monomers and the overall degree of regioregularity is about 20%. After an energy minimization step, we performed NPT simulations for the chains at 700 K and 1 bar over 30 ns to obtain isotropic melts. The melts were quenched to 300 and 350 K and simulated for 20 ns using velocity rescaling thermostat and Parrinello–Rahman barostat so that the densities of the samples fluctuated about steady values. The densities of regiorandom P3HT and P3DDT are 1.05 and 0.98 g/cm^3 at 300 K and 1.03 and 0.96 g/cm^3 at

350 K. Predicted densities are compared with densities measured in a parallel plate geometry as previously described,[39] and although we find our predictions are consistently lower than experimental results, values are within 5% (Supporting Information Fig. S2). Extra NPT simulations of 20 ns were performed for the equilibrated samples, from which we measured the mean-square displacements of the hydrogen atoms. In all of our simulations, the van der Waals interactions are cut-off at 1.2 nm and Coulombic interactions are treated using Particle Mesh Ewald (PME) method. By comparing the motions of atoms sampled from different periods of our simulations, we ensured that the systems were in equilibrium.

NMR Experiments

^{13}C MAS spectra were collected on a Bruker Avance 500 spectrometer with a field of 11.7 T and at a spinning speed of 20 kHz. The standard Torchia pulse sequence was applied for T_1 measurements, using nine delay times per temperature.[40] The spectra were apodized using an exponential function (30 Hz decay) to enhance the signal to noise ratio. After Fourier transformation, the peaks were fitted to Voigt functions to deconvolute overlapping peaks. Then non-overlapping peaks were fitted to an exponential decay function, from which the T_1 relaxation time was determined.

RESULTS AND DISCUSSION

MD Simulation Results

Using MD simulations, we can examine the role of side chains on the motion of the backbone of P3ATs. The amorphous melts are composed of 64 chains of regiorandom P3HT and P3DDT with 20 repeat units. Predicted densities are within 5% of experimentally measured values (Supporting Information Fig. S2). We ensure that our isotropic melts are equilibrated by comparing the motions of atoms sampled from different time periods of our simulations.

The values for the mean-square displacement (MSD) at 2 ns for the hydrogen atoms in regiorandom P3HT and P3DDT at 300 and 350 K are shown in Figure 2. MSDs as a function of time are shown in Supporting Information Figure S3. The time scale was chosen to match to QENS experiments discussed later. For both P3HT and P3DDT, the MSD increases as the carbon atom moves away from the backbone (i.e., the hydrogen index in Fig. 1 increases). The MSD also increases with temperature, as expected.

Our simulations also predict that longer side chains can lead to faster motions for polymer backbones. As the side chain length increases from hexyl to dodecyl, the motions of atoms on thiophene rings (hydrogen index = 0) are enhanced at both 300 and 350 K. Thus, the side chains plasticize the backbone.

Small-Angle Neutron Scattering

Using small-angle neutron scattering (SANS), we examine the static structure of regiorandom P3ATs. Figure 3 shows SANS intensities versus scattering vector q (q = $2\pi/d$, where d is the spacing between domains). High intensities are apparent at
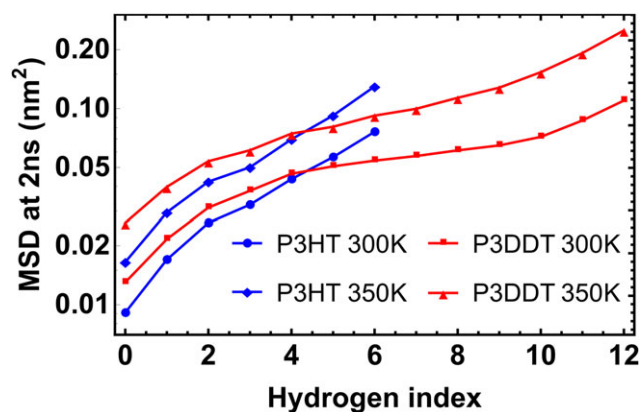
FIGURE 2 Mean-square displacement (MSD) of hydrogen at 2 ns. Index 0 for ring hydrogen. Indices through 6 and 12 for hydrogen on side chain ends of P3HT and P3DDT, respectively. [Color figure can be viewed at wileyonlinelibrary.com]

low q, which could be due to dust or porosity from sample preparation.

The SANS data for all P3ATs also show broad peaks near $q = 0.2$ to 0.5 1/Å, suggesting that all samples are amorphous at 300 K. The alkyl side chains have more protons than the thiophene backbones, such that the scattering contrast in SANS will be mostly between side chains and aromatic backbones. Furthermore, the spacing corresponds to 10–30 Å, or roughly the expected distance between backbones across the side chains. Thus, the peaks in Figure 3 are indicative of microphase separation between the backbone and the side chains, consistent with previous reports.[14,21,41–43]

As a consequence of microphase separation between the side chains and backbones, we speculate that the increase in inter-chain spacing observed in Figure 3 does not directly affect charge transport. Amorphous poly(3-alkylthiophene)s often exhibit two amorphous halos in scattering experiments.[43]
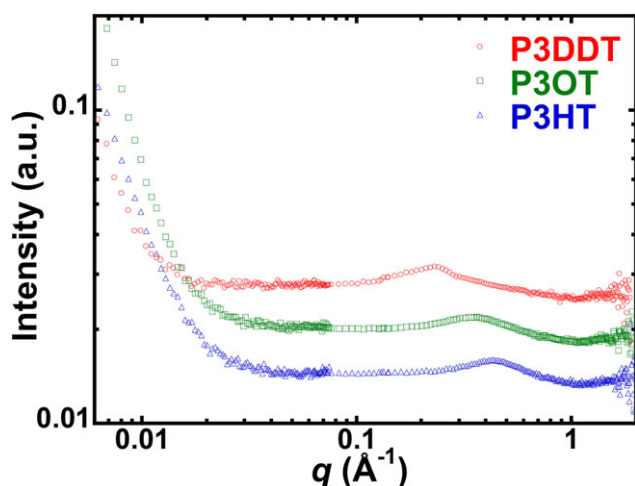
These two scattering features denote a close distance between backbones, presumably within microphase separated domains, and a longer distance between chains but across side chains. Because charge hopping across side chains is negligible due to the large distances (>1 nm), perturbing this distance should have no effect on macroscopic charge transport.

Thermal Transitions in Regiorandom P3ATs

The enhanced chain motion predicted from MD simulations will result in a drop in the glass transition temperature (T_g). We measured thermal transitions, including glass transitions and side chain melting, using differential scanning calorimetry (DSC) for regiorandom P3ATs. Figure 4 shows the DSC thermograms of regiorandom P3ATs. For P3DDT, a heat capacity peak is apparent around 20°C, corresponding to a melting transition of the dodecyl side-chains. The absence of side chain melting peak for P3HT and P3OT suggests that shorter alkyl side-chains are amorphous even below room temperature.

Nevertheless, we can extract the T_g from the drop in heat capacity as temperature decreases from 10 to −30°C for all P3ATs. The T_gs for regiorandom P3HT, P3OT, and P3DDT are 6, −17, and −26°C, respectively, although the T_g for regiorandom P3DDT is challenging to determine from DSC due to the overlap of the glass transition with the side chain melting peaks. The decreasing T_g suggests that the polymer mobility increases as side-chain length increases, and corroborates our results from MD simulations.

Solid State NMR Measurements

We also qualitatively demonstrate that the motions of side chain atoms are enhanced away from the backbones using solid state NMR relaxation, which can probe the motions of individual atoms within a molecule. This is possible because spin-lattice (T_1) relaxation is driven by coupling to thermal lattice vibrations, occurring at the Larmor frequency, as
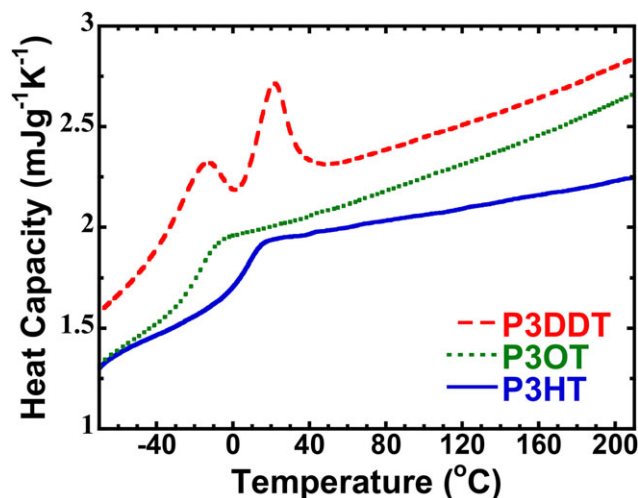

FIGURE 3 SANS profiles of P3ATs at 300 K. [Color figure can be viewed at wileyonlinelibrary.com]

FIGURE 4 DSC heating scan for regiorandom P3ATs. [Color figure can be viewed at wileyonlinelibrary.com]

described by BPP theory.[44] Raw solid state NMR spectra are shown in Supporting Information Figure S4.

Assuming that nuclear motions are isotopic, one can write an autocorrelation function of form e, where τ_c is the correlation time, which represents the timescale on which the orientation of nuclei changes by 1 radian. The correlation time is related to the T_1 relaxation rate by:

$$\frac{1}{T_1} = K \frac{\tau_c}{1 + \omega_0^2 \tau_c^2} + \frac{2\tau_c}{1 + 4\omega_0^2 \tau_c^2} \tag{1}$$

in which T_1 is the spin-lattice relaxation time and ω_0 is the Larmor frequency. This relationship indicates that T_1 reaches a minimum when the correlation time is equal to the inverse of ω_0. Observation of this T_1 minimum is required to convert relaxation times to correlation times, due to the presence of the proportionality constant K in eq 1. Nevertheless, even if no T_1 minimum is observed, by measuring the change in T_1 as a function of temperature, we can determine whether the side chain vibrations occur at timescales slower or faster than ω_0^{-1}. Figure 5 shows the solid state ^{13}C T_1 relaxation time as a function of temperature for the side chain carbons of RRa-P3HT. For atoms that are close to the polymer backbone (C_{1-3}), T_1 does not change over the temperature range from 250 to 340 K. Our result is consistent with a previous study of regioregular P3HT, in which a broad T_1 minimum was found, corresponding to a τ_c of order 8 ns.[45]

For the end carbons, C_4, C_5, and C_6, we observe that the values of T_1 increase with increasing temperature, indicating the values of τ_c become smaller than ω_0^{-1}, which is 8 ns. Computing the exact correlation time τ_c, however, can be rather ambiguous, because no T_1 minimum is observed in the temperature range from 250 to 340 K. Nonetheless, linear fits to T_1 data indicate that the slopes are positive with at least a 95% confidence interval. The smaller τ_c values for C_4, C_5, and C_6 indicate enhanced motions of the carbons atoms further away from the rigid backbone. This result is consistent with our MD simulations.

Quasi-Elastic Neutron Scattering

We probed dynamics at different length scales (different q values) using QENS. We expect that aromatic backbones are much slower than alkyl side chains, such that QENS may be able to resolve individual contributions to chain dynamics in P3ATs.

Other techniques, such as Dielectric Relaxation Spectroscopy (DRS), can be also used to measure dynamics. Information obtained from DRS, however, includes both the contributions from side-chains and backbones. It is impossible to distinguish the motions of backbones from the side-chains unless their frequencies are well separated.[19,46,47]

Figure 6 shows the total elastic intensity summed over various q as a function of temperature. All data are normalized to
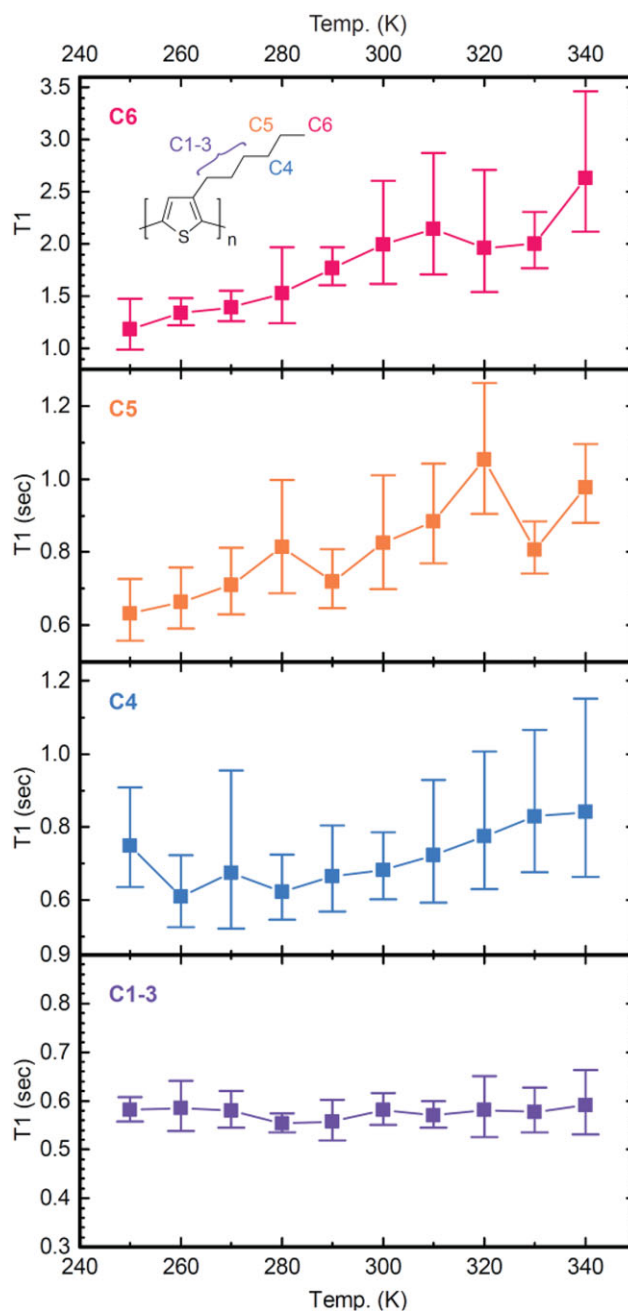

FIGURE 5 Temperature dependent solid-state NMR relaxation measurements of RRa-P3HT. Plots show ^{13}C T_1 relaxation time as a function of temperature for the indicated side chain atoms. Inset: carbon atom index (numbering scheme). [Color figure can be viewed at wileyonlinelibrary.com]

1 at 100 K. The elastic intensities decay as temperature increases from enhanced segmental motion of the backbone or side chains. The elastic intensity is calculated by summing the signals within the energy resolution of the instrument, such that when the time scale of segmental motions is below the resolution, the elastic intensity drops. Near 250–300 K, a change in slope in the elastic intensity and the MSD is apparent and corresponds to the glass transition. The change in slope is most apparent in P3DDT, and we attribute this to
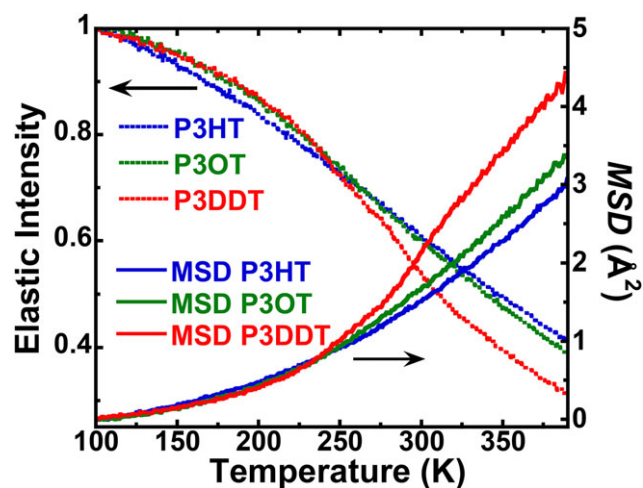
FULL PAPER

WWW.POLYMERPHYSICS.ORG

JOURNAL OF
POLYMER SCIENCE

Polymer
Physics

FIGURE 6 (Left) Total elastic intensity (sum over 16 scattering vectors) as a function of temperature. Data is normalized to 1 at 100 K. (Right) Ensemble averages of the MSD of P3ATs as a function of temperature. [Color figure can be viewed at wileyonlinelibrary.com]

contributions both from the glass transition and the melting of the side chains near 300 K shown in Figure 4.

When vibrational motions dominate the dynamics of polymers, the elastic intensity I can be described using the Debye–Waller Factor: $I = \exp(-q^2 <u^2>/3)$, where $<u^2>$ is the mean-square-displacement.[48] We therefore assume that the ensemble average of mean-square-displacement of all the protons can be calculated as the slope of $-3\ln[I(T)/I(T_{min})]$ versus q^2.[49] At low temperatures, the mean-square-displacements of P3ATs increase linearly as temperature increases (Figure 6).

Between 260 and 295 K, as a result of the glass transition, the mean-square-displacements start to deviate from the linear trends at lower temperatures (Figure 6). The larger values of the mean-square-displacement of P3DDT indicate that the accessible length scale of the alkyl side-chains is higher for P3DDT than P3OT and P3HT. At temperatures above 300 K, the mean-square-displacements again increase linearly with temperature, but with larger slopes than at low temperatures (<200 K).

We also performed dynamic scans for P3ATs at 300 and 350 K, where the side-chains are fully mobile. In dynamic scans, the incident neutrons exchange their kinetic energy with the mobile molecules and the instrument detects the change in neutron energy before and after scattering. Larger changes in neutron energy are a result of faster molecular motions.

The dynamics of P3ATs can be inferred from the scattering intensity S(q,ω), which is a function of both the energy change (ω) and the momentum transfer (q). As shown in Figure 7(a), the instrument resolution represents S(q,ω) for an immobile system (100% elastic scattering). The peak around zero

energy transfer is a result of elastic scattering and the broadening of the elastic signal (quasi-elastic scattering) arises from the translational, vibrational, and rotational motions in the samples. The broadness of the scattering peak is governed by the relaxation time of the motions in the sample, such that broader peaks indicate shorter relaxation times and faster motion.

We observe that the longer alkyl side chains of P3ATs can move faster. The broadness of the quasi-elastic scattering signal (intensities at ω ≠ 0) increases at 300 K as the side chain increases from hexyl to dodecyl, as shown in Figure 7(a). Because the rigid polythiophene backbones are slower (with a higher glass transition temperature) than the alkyl side chains, the slow motions of the backbones can suppress the mobility of side chains. As the side-chain length increases, the effect of suppression became less prominent in P3ATs.
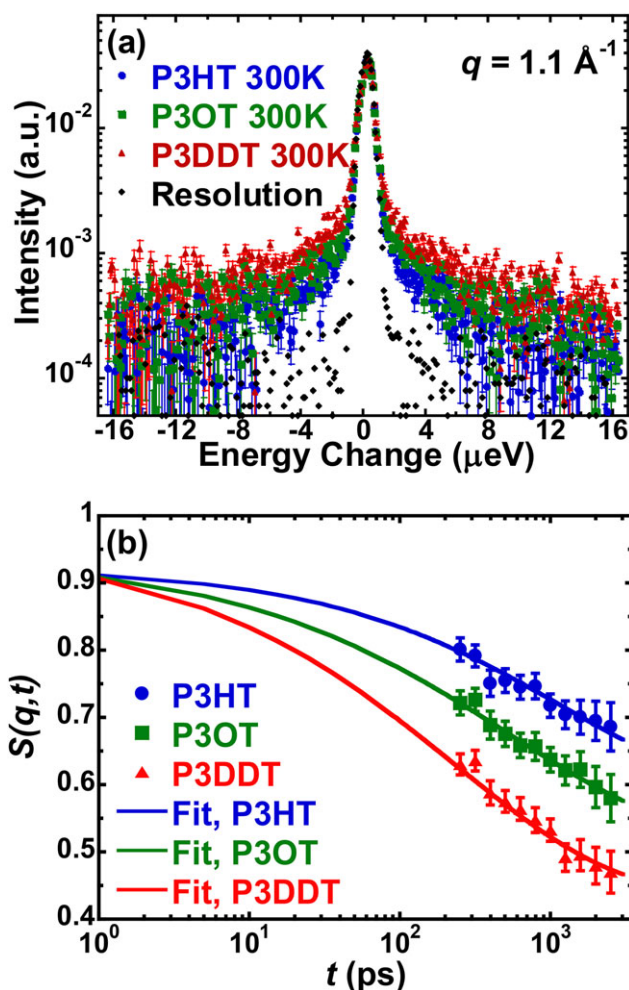

FIGURE 7 (a) S(q,ω) of P3HT (blue triangle), P3OT (green rectangular), P3DDT (red circle), and instrument resolution (Black dashed line) at 300 K and momentum transfer of 1.1 Å⁻¹. (b) S(q,t) of P3HT (empty triangle), P3OT (empty rectangular), and P3DDT (empty circle) at 300 K and momentum transfer of 1.1 Å⁻¹. Solid curves are the KWW fits. [Color figure can be viewed at wileyonlinelibrary.com]

We inverse Fourier transform the scattering function in frequency domain $S(q,\omega)$ to obtain the intermediate scattering function $S(q,t)$ in the time domain. $S(q,t)$ is the self-autocorrelation function of protons in reciprocal space. A faster decay of $S(q,t)$ suggests a faster relaxation process. We show $S(q,t)$ in Figure 7(b) for the three regiorandom P3AT samples at $q = 1.1$ Å^{-1}, $S(q,t)$ at various q are also shown in Supporting Information Figures S5–S10. The decay of $S(q,t)$ becomes more significant as the side-chain length increases.

To quantitatively describe the motions of protons in P3ATs, we fit $S(q,t)$ to a combination of two Kolrausch–Williams–Watts (KWW) equations:

$$S(q,t) = (x\text{KWW}_{rot} + 1 - x)\text{KWW}_{trans} \qquad (2)$$

in which x is the fraction of hydrogen atoms in the methyl group with respect to all of the hydrogen atoms in the system, KWW_{trans} and KWW_{rot} represents the translational diffusion of protons and the rotation of protons in the methyl groups, respectively. In regiorandom P3ATs, the protons in the methyl groups can undergo both translational diffusion and three-fold rotation.

The KWW equation is a stretched exponential function:[50]

$$\text{KWW} = \text{EISF}(q) + (1 - \text{EISF}[q])) e^{-\left(\frac{t}{\tau(q)}\right)^{\beta(q)}} \qquad (3)$$

where, τ is the relaxation time of the process, β is the stretch factor and represents the distribution of the relaxation time, and EISF is the elastic incoherent structure factor, governed by the fraction of protons that are not mobile. The q dependence of EISF can be used to describe the shape of a type of motion.[26]

For the rotational motions, we set the stretch factor β_{rot} in KWW to unity for all temperatures and momentum transfers, because all the protons in the methyl group are equivalent. The EISF_{rot} is derived theoretically from a three-fold rotation with equal probability model.[26] The only fitting parameter for the rotational motions is therefore the relaxation time τ_{rot}. In fact, our fitting suggests that τ_{rot} remains constant at different q, as expected for the q dependence of the rotational relaxation (Supporting Information Fig. S11).

We do not include the contributions of vibrational motions in our $S(q,t)$ fit, although such motions exist in regiorandom P3ATs. This is because the time scale of molecular vibrations is completely out of the instrument time window, and are not captured by the high-flux backscattering spectrometer in dynamic scans.

We obtain the EISF for translational motions as a fitting parameter from the scattering function in time domain $S(q,t)$. Relaxation times τ and stretch factors β are shown in Supporting Information Figures S12 and S13. The q dependence of

EISF, which quantifies the shape of the motions, is plotted in Figure 8. The value of the EISF decreases as q decreases. By varying the side chain length from hexyl to dodecyl, the decay of EISF becomes more significant, indicating the enhanced length scale for side-chain motions.

The shapes of proton motions can be obtained by fitting the q dependence of EISF with theoretical models. For proton diffusion in small molecules such as water, a sphere of radius R is commonly used to define the spatial range of the motion.[51,52] In P3ATs, however, the translational motions of protons vary along the side-chains, which is reflected in the stretch factor β_{trans} that is smaller than unity.

Instead of using a single sphere to describe the geometry of proton motions in P3ATs, we use a series of spheres with different radius R_n. In this way, we treat the motions of different proton sites along the side chains separately. Figure 8(a) is a schematic representation of the extent of motion as "dynamic" spheres for P3HT. Seven, nine and thirteen spheres ($N = 7$, 9, 13) are assigned to P3HT, P3OT, and P3DDT, respectively.

The total EISF(q) of protons can be calculated as the summation of theoretical $\text{EISF}_n(q)$ over all the spheres:

$$\text{EISF}(q) = \sum_1^N x_n \text{EISF}_n(q) \qquad (4)$$

$$\text{EISF}_n(q) = \left[\frac{3 j_1(q R_n)}{q R_n}\right]^2 \qquad (5)$$

$$j_1(q R_n) = \frac{\sin(q R_n) - (q R_n)\cos(q R_n)}{(q R_n)^2} \qquad (6)$$

in which n is the index of the sphere (we define n = 0 for the α-protons on the thiophene ring), x_n is the fraction of the overall protons in the nth sphere, and N is the total number of spheres.

For P3ATs, we expect a clear variation in the translational dynamics of the protons along the side chains (from the α-protons to protons in the end methyl groups). The mobility of atoms close to the backbones is suppressed because of the slow motions of the stiff backbones. The suppression of mobility may decay along the side chain so that if the alkyl side-chain is long enough, the end methyl group will have the same dynamical behaviors as polyethylene.

As suggested in previous QENS studies of alkyl side-chains in other soft materials,[46,53,54] the radius of spheres R_n may increase linearly as n increases. To validate this model for P3ATs, we fit our EISF using spheres with radius of $R_n = R_0 + C\,n^h$. R_0 is the radius of the sphere for the hydrogen on the thiophene ring, governed by the amplitude of ring motions. C is a constant that characterizes the linear variation in R_n. h is an exponent that we set to 1 to represent linear growth in motion along the side chain and away from the backbone.
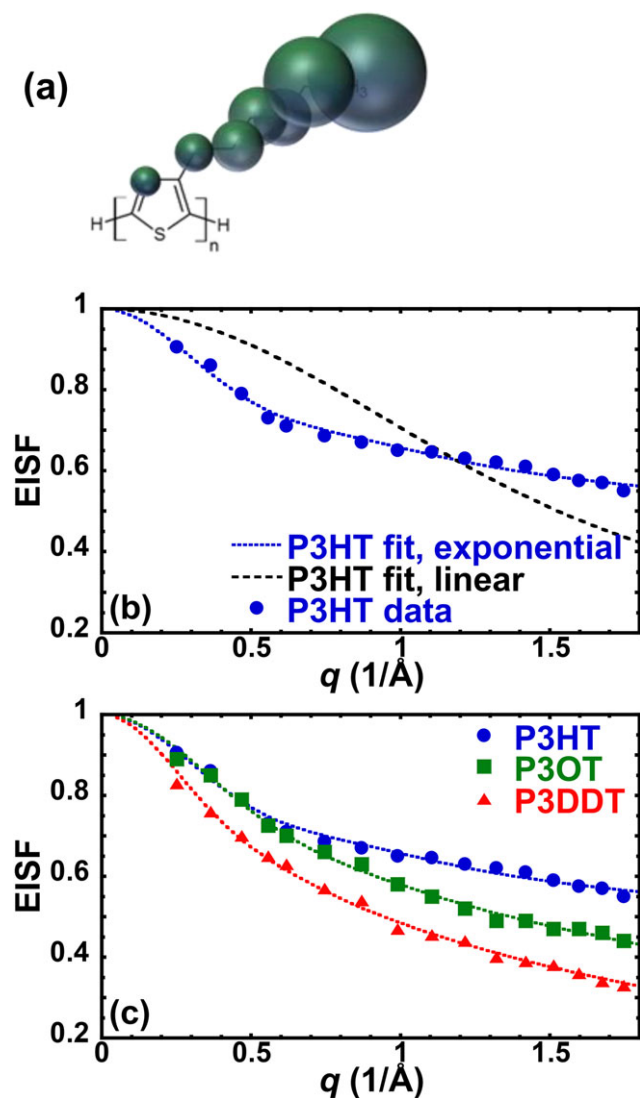
FULL PAPER

WWW.POLYMERPHYSICS.ORG

JOURNAL OF
POLYMER SCIENCE

Polymer
Physics

$$R_n = R_0 \gamma^n \qquad (7)$$

in which R_0 is the radius of the sphere assigned to the proton on the thiophene ring, γ is an exponential factor that characterizes the change in R_n, such that a larger γ value indicates less correlation in molecular motions for adjacent spheres. Figure 8(c) shows that our exponential model can provide a good qualitative fit for EISF(q) with γ values shown in Supporting Information Table S2. The values of γ decrease as the side chains become shorter, suggesting motions of the carbon atoms in the side chains are less correlated for longer side chains. We speculate that when side chains are longer, on average motion of the alkyl groups is less restricted by the stiff backbone, thereby leading to less correlated motion along the side chains.

The results of R_n versus carbon position at 300 K are shown in Figure 9(a). The match between MD simulations and QENS results is qualitative, where an increase in motion of the hydrogen on the thiophene backbone with increasing side chain length is apparent in both sets of results. The lack of
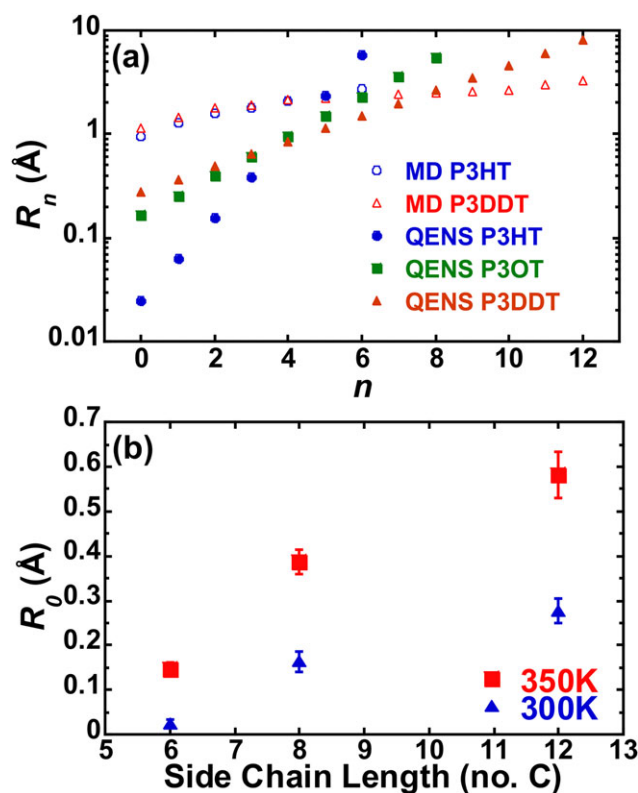
FIGURE 8 (a) Schematic for diffusion model of side chains of P3HT. A sphere is assigned to each proton site. (b) EISF of regiorandom P3HT at 300 K (dots). Fit from exponential model (dotted blue line) and linear model (dashed black line). (c) EISF of P3ATs at 300 K. Dotted lines represent fits with an exponential model. [Color figure can be viewed at wileyonlinelibrary.com]

The fit quality of the linear model, however, is poor. The black dashed line in Figure 8(b) is the best fit of the P3HT EISF at 300 K with the linear model (more attempts to fit the EISF are shown in the Supporting Information Figs. S14–S16). Thus, the sphere radius R_n may not grow linearly for the motions of protons on alkyl side chains in P3ATs. Furthermore, increasing the exponent h to 2 and 3 also yield poor fits (Supporting Information Figs. S15 and S16).

Our MSDs from MD simulations shown in Figure 2 and NMR relaxometry in Figure 5 show that motion increases away from the backbone along the side chain. The MD simulations suggest that the increase in motion is roughly exponential with increasing hydrogen index. Thus, we assume the radius of spheres increases exponentially:

FIGURE 9 (a) Sphere radius that is proportional to the extent of motion of hydrogens attached to various carbon atoms as defined by the index n described in the text. Results are shown from MD simulations and QENS experiments. (b) Radius of sphere of proton on thiophene ring, which is proportional to the extent of motion of the hydrogen on the thiophene rings and, therefore, the backbone, at 300 and 350 K from QENS experiments. [Color figure can be viewed at wileyonlinelibrary.com]

quantitative agreement can be due to a number of factors. QENS results are extracted by modeling the extent of hydrogen motion as spheres, even though the motion could be anisotropic. Furthermore, the force fields used in MD simulations may not be finely tuned to capture the dynamics of P3ATs in quantitative detail. Nevertheless, there are various conclusions that are consistent between simulations and experiments. The extent of motion of hydrogens on the terminal carbon (methyl group) is approximately the same for all three polymers in both MD simulations and QENS results. Furthermore, the radius of the sphere corresponding to the hydrogen attached to the backbone (R_0) increases with increasing alkyl side chain length.

We plot R_0 as a function of side chain length in Figure 9(b). The value of R_0 represents the amplitude of dynamic fluctuations for conjugated backbones. We observe that the spatial range of the motions for the thiophene rings increases as the side chain length increases, consistent with our MD simulation results (Fig. 2).

Polyethylene chains are flexible, and can relax on a time scale of picoseconds, much shorter than the relaxation times of stiff polythiophenes.[46,55] As a consequence, the fast motions of alkyl side chains, which are essentially polyethylene oligomers, can enhance the mobility of the thiophene backbones. Thus, side chains can plasticize the aromatic backbones of conjugated polymers. Similarly, increasing the length of side chains in poly(alkyl methacrylates) has been demonstrated to lower the glass transition temperature and increase backbone mobility.[56–58]

CONCLUSIONS

In this work, we combine MD simulations with neutron scattering experiments to study the effect of alkyl side-chains on the structure and segmental dynamics of regiorandom P3ATs. Using simulations, we obtain the short time dynamics of atoms in the amorphous samples of P3HT and P3DDT. We predict that increasing side chain length can enhance the mobility of thiophene backbones.

To validate our predictions, we probe the polymer segmental dynamics using QENS. We observe that the alkyl side chain mobility is indeed higher in regiorandom P3ATs with longer side chains. The motions are faster for atoms away from the backbones. By fitting the quasi-elastic signals, we show that the faster motions of side chains can lead to a higher mobility for the thiophene backbones. By performing solid state NMR measurements for P3HT, we also qualitatively validate our results.

Because the charge mobility in amorphous materials is limited by inter-chain charge hopping, the enhanced motions of polymer backbones may affect the distribution of π–π stacking distance over time, and in turn affect the electronic coupling between conjugated rings. Nonetheless, the role of segmental dynamics on charge transport of soft semiconductors is still not well understood. Future work correlating the dynamics on different time scales with chage mobilities of conjugated polymers is warranted, to better understand the role of thermal fluctuations on charge transport.

REFERENCES AND NOTES

1 H. Sirringhaus, *Adv. Mater.* **2005**, *17*, 2411.

2 J. E. Anthony, *Chem. Rev.* **2006**, *106*, 5028.

3 Y. Lee, E. D. Gomez, *Macromolecules* **2015**, *48*, 7385.

4 S. R. Forrest, *Nature* **2004**, *428*, 911.

5 H. Sirringhaus, P. J. Brown, R. H. Friend, M. M. Nielsen, K. Bechgaard, B. M. W. Langeveld-Voss, A. J. H. Spiering, R. A. J. Janssen, E. W. Meijer, P. Herwig, D. M. de Leeuw, *Nature* **1999**, *401*, 685.

6 I. McCulloch, M. Heeney, C. Bailey, K. Genevicius, I. Macdonald, M. Shkunov, D. Sparrowe, S. Tierney, R. Wagner, W. Zhang, M. L. Chabinyc, R. J. Kline, M. D. McGehee, M. F. Toney, *Nat. Mater.* **2006**, *5*, 328.

7 I. Osaka, R. Zhang, G. Sauve, D. M. Smilgies, T. Kowalewski, R. D. McCullough, *J. Am. Chem. Soc.* **2009**, *131*, 2521.

8 D. S. Chung, S. J. Lee, J. W. Park, D. B. Choi, D. H. Lee, J. W. Park, S. C. Shin, Y. H. Kim, S. K. Kwon, C. E. Park, *Chem. Mater.* **2008**, *20*, 3450.

9 W. M. Zhang, J. Smith, S. E. Watkins, R. Gysel, M. McGehee, A. Salleo, J. Kirkpatrick, S. Ashraf, T. Anthopoulos, M. Heeney, I. McCulloch, *J. Am. Chem. Soc.* **2010**, *132*, 11437.

10 V. Coropceanu, J. Cornil, D. A. da Silva Filho, Y. Olivier, R. Silbey, J.-L. Brédas, *Chem. Rev.* **2007**, *107*, 926.

11 H. Sirringhaus, M. Bird, T. Richards, N. Zhao, *Adv. Mater.* **2010**, *22*, 3893.

12 J. Colmenero, A. Alegra, J. M. Alberdi, F. Alvarez, B. Frick, *Phys. Rev. B* **1991**, *44*, 7321.

13 B. Farago, C. X. Chen, J. K. Maranas, S. Kamath, R. H. Colby, A. J. Pasquale, T. E. Long, *Phys. Rev. E* **2005**, *72*,

14 A. Babel, S. A. Jenekhe, *Synth. Met.* **2005**, *148*, 169.

15 G. Sauve, A. E. Javier, R. Zhang, J. Y. Liu, S. A. Sydlik, T. Kowalewski, R. D. McCullough, *J. Mater. Chem.* **2010**, *20*, 3195.

16 K. Vakhshouri, E. D. Gomez, *Macromol. Rapid Commun.* **2012**, *33*, 2133.

17 T. Liu, A. Troisi, *Adv. Funct. Mater.* **2014**, *24*, 925.

18 A. A. Y. Guilbert, A. Urbina, J. Abad, C. Díaz-Paniagua, F. Batallán, T. Seydel, M. Zbiri, V. García-Sakai, J. Nelson, *Chem. Mater.* **2015**, *27*, 7652.

19 J. Obrzut, K. A. Page, *Phys. Rev. B* **2009**, *80*, 211.

20 Y. D. Park, D. H. Kim, Y. Jang, J. H. Cho, M. Hwang, H. S. Lee, J. A. Lim, K. Cho, *Org. Electron.* **2006**, *7*, 514.

21 W. D. Oosterbaan, J. C. Bolsee, A. Gadisa, V. Vrindts, S. Bertho, J. D'Haen, T. J. Cleij, L. Lutsen, C. R. McNeill, L. Thomsen, J. V. Manca, D. Vanderzande, *Adv. Funct. Mater.* **2010**, *20*, 792.

22 R. Noriega, J. Rivnay, K. Vandewal, F. P. Koch, N. Stingelin, P. Smith, M. F. Toney, A. Salleo, *Nat. Mater.* **2013**, *12*, 1038.

23 T. J. Prosa, M. J. Winokur, J. Moulton, P. Smith, A. J. Heeger, *Macromolecules* **1992**, *25*, 4364.

24 K. Vakhshouri, D. R. Kozub, C. Wang, A. Salleo, E. D. Gomez, *Phys. Rev. Lett.* **2012**, *108*, 026601.

25 J. K. Zhao, C. Y. Gao, D. Liu, *J. Appl. Crystallogr.* **2010**, *43*, 1068.

26 Bée, M, *Quasielastic Neutron Scattering: Principles and Applications in Solid State Chemistry, Biology, and Materials Science*; Adam Hilger: Bristol, England; Philadelphia, **1988**.

27 V. G. Sakai, C. X. Chen, J. K. Maranas, Z. Chowdhuri, *Macromolecules* **2004**, *37*, 9975.

28 L. V. N. R. Ganapatibhotla, J. K. Maranas, *Macromolecules* **2014**, *47*, 3625.

29 A. Meyer, R. M. Dimeo, P. M. Gehring, D. A. Neumann, *Rev. Sci. Instrum.* **2003**, *74*, 2759.

30 R. T. Azuah, L. R. Kneller, Y. M. Qiu, P. L. W. Tregenna-Piggott, C. M. Brown, J. R. D. Copley, R. M. Dimeo, *J. Res. Natl. Inst. Std. Technol.* **2009**, *114*, 341.

31 H. J. C. Berendsen, D. van der Spoel, R. van Drunen, *Comput. Phys. Commun.* **1995**, *91*, 43.

32 D. M. Huang, R. Faller, K. Do, A. Moule, *J. Chem. Theory Comput.* **2010**, *6*, 526.

33 K. N. Schwarz, T. W. Kee, D. M. Huang, *Nanoscale* **2013**, *5*, 2017.

34 W. L. Jorgensen, D. S. Maxwell, J. Tirado-Rives, *J. Am. Chem. Soc.* **1996**, *118*, 11225.

35 W. L. Zhang, E. D. Gomez, S. T. Milner, *Macromolecules* **2014**, *47*, 6453.

36 W. Zhang, E. D. Gomez, S. T. Milner, *Macromolecules* **2015**, *48*, 1454.

37 B. McCulloch, V. Ho, M. Hoarfrost, C. Stanley, C. Do, W. T. Heller, R. A. Segalman, *Macromolecules* **2013**, *46*, 1899.

38 V. Ho, B. W. Boudouris, R. A. Segalman, *Macromolecules* **2010**, *43*, 7895.

39 R. Xie, Y. Lee, M. P. Aplan, N. J. Caggiano, C. Müller, R. H. Colby, E. D. Gomez, *Macromolecules* **2017**, *50*, 5146.

40 D. A. Torchia, *J. Magn. Reson.* **1978**, *30*, 613.

41 G. M. Newbloom, S. M. Hoffmann, A. F. West, M. C. Gile, P. Sista, H. K. C. Cheung, C. K. Luscombe, J. Pfaendtner, L. D. Pozzo, *Langmuir* **2015**, *31*, 458.

42 G. M. Newbloom, P. de la Iglesia, L. D. Pozzo, *Soft Matter* **2014**, *10*, 8945.

43 C. Wang, J. Rivnay, S. Himmelberger, K. Vakhshouri, M. F. Toney, E. D. Gomez, A. Salleo, *ACS Appl. Mater. Interf.* **2013**, *5*, 2342.

44 N. Bloembergen, E. M. Purcell, R. V. Pound, *Phys. Rev.* **1948**, *73*, 679.

45 K. Yazawa, Y. Inoue, T. Shimizu, M. Tansho, N. Asakawa, *J. Phys. Chem. B* **2010**, *114*, 1241.

46 J. K. Maranas, *Curr. Opin. Colloid Interf. Sci.* **2007**, *12*, 29.

47 S. A. Chen, C. S. Liao, *Macromolecules* **1993**, *26*, 2810.

48 C. Kittel, *Introduction to Solid State Physics*; Wiley: New York, NY, **1976**.

49 S.-H. Chen, L. Liu, E. Fratini, P. Baglioni, A. Faraone, E. Mamontov, *Proc. Natl. Acad. Sci.* **2006**, *103*, 9012.

50 G. Williams, D. C. Watts, *Trans. Faraday Soc.* **1970**, *66*, 80.

51 F. Volino, M. Pineri, A. J. Dianoux, A. De Geyer, *J. Polym. Sci. Part B: Polym. Phys.* **1982**, *20*, 481.

52 M. Doxastakis, V. G. Sakai, S. Ohtake, J. K. Maranas, J. de Pablo, *Biophys. J.* **2007**, *92*, 147.

53 M. Trapp, T. Gutberlet, F. Juranyi, T. Unruh, B. Deme, M. Tehei, J. Peters, *J. Chem. Phys.* **2010**, *133*, 164505.

54 V. K. Sharma, S. Mitra, G. Verma, P. A. Hassan, V. G. Sakai, R. Mukhopadhyay, *J. Phys. Chem. B* **2010**, *114*, 17049.

55 V. G. Sakai, J. K. Maranas, I. Peral, J. R. D. Copley, *Macromolecules* **2008**, *41*, 3701.

56 S. Farhangi, H. Weiss, J. Duhamel, *Macromolecules* **2013**, *46*, 9738.

57 O. F. Pascui, D. Reichert, *Appl. Magn. Reson.* **2004**, *27*, 419.

58 M. R. Hansen, R. Graf, H. W. Spiess, *Chem. Rev.* **2016**, *116*, 1272.